HHS Public Access

Author manuscript

FASEB J. Author manuscript; available in PMC 2021 November 01.

Published in final edited form as:

FASEB J. 2020 November ; 34(11): 14750–14767. doi:10.1096/fj.202000850RR.

Small ubiquitin-like modifier 2 (SUMO2) is critical for memory processes in mice

Shu Yu[1,2,†], **Francesca Galeffi**[3,4,†], **Ramona M. Rodriguiz**[5,†], **Zhuoran Wang**[1], **Yuntian Shen**[1,2], **Jingjun Lyu**[1], **Ran Li**[1], **Joshua D. Bernstock**[6], **Kory R. Johnson**[7], **Shuai Liu**[1], **Huaxin Sheng**[1], **Dennis A. Turner**[3,4], **William C. Wetsel**[5,8], **Wulf Paschen**[1], **Wei Yang**[1]

[1]Department of Anesthesiology, Duke University Medical Center, Durham, NC, USA

[2]Key Laboratory of Neuroregeneration of Jiangsu and Ministry of Education, Co-Innovation Center of Neuroregeneration, Nantong University, Nantong, China

[3]Research and Surgery Services, Durham VAMC, Durham, NC, USA

[4]Departments of Neurosurgery, Neurobiology, and Biomedical Engineering, Duke University Medical Center, Durham, NC, USA

[5]Department of Psychiatry and Behavioral Sciences, Mouse Behavioral and Neuroendocrine Analysis Core Facility, Duke University Medical Center, Durham, NC, USA

[6]Stroke Branch, National Institute of Neurological Disorders and Stroke, National Institutes of Health (NINDS/NIH), Bethesda, MD, USA

[7]Bioinformatics Section, National Institute of Neurological Disorders and Stroke, National Institutes of Health (NINDS/NIH), Bethesda, MD, USA

[8]Departments of Neurobiology and Cell Biology, Duke University Medical Center, Durham, NC, USA

Abstract

Small ubiquitin-like modifier (SUMO1–3) conjugation (SUMOylation), a post-translational modification, modulates almost all major cellular processes. Mounting evidence indicates that SUMOylation plays a crucial role in maintaining and regulating neural function, and importantly its dysfunction is implicated in cognitive impairment in humans. We have previously shown that simultaneously silencing SUMO1–3 expression in neurons negatively affects cognitive function. However, the roles of the individual SUMOs in modulating cognition and the mechanisms that link SUMOylation to cognitive processes remain unknown. To address these questions, in this study, we have focused on SUMO2 and generated a new conditional *Sumo2* knockout mouse line. We found that conditional deletion of *Sumo2* predominantly in forebrain neurons resulted in

Correspondence to: Wulf Paschen PhD or Wei Yang PhD, Department of Anesthesiology, Duke University Medical Center, Box 3094, Research Drive, Durham, NC 27710, USA; phone: 919-684-6573; wulf.paschen@duke.edu; wei.yang@duke.edu.

Author Contributions: DAT, WCW, WP, and WY designed research; SY, FG, RMR, JDB, KRJ, DAT, WCW, WP, and WY analyzed data; SY, FG, RMR, ZW, YS, RL, JL, SL, HS, and WY performed research; SY, FG, RMR, DAT, WCW, WP, and WY wrote the paper.

[†]These authors contributed equally to this work.

Conflict of interest.

The authors declare that they have no conflict of interest.

marked impairments in various cognitive tests, including episodic and fear memory. Our data further suggest that these abnormalities are attributable neither to constitutive changes in gene expression nor to alterations in neuronal morphology, but they involve impairment in dynamic SUMOylation processes associated with synaptic plasticity. Finally, we provide evidence that dysfunction on hippocampal-based cognitive tasks was associated with a significant deficit in the maintenance of hippocampal long-term potentiation in *Sumo2* knockout mice. Collectively, these data demonstrate that protein conjugation by SUMO2 is critically involved in cognitive processes.

Keywords

post-translational modification; LTP; knockout; memory impairment

Introduction

Memory formation via synaptic plasticity requires the concerted action of many molecular and cellular processes including gene regulation, mRNA splicing, protein synthesis and trafficking, neurotransmitter release, and signal transduction (1). These processes can be regulated by post-translational modifications, which rapidly and reversibly modulate the functions and localizations of pre-existing proteins. For example, protein phosphorylation plays an essential role in many aspects of synaptic plasticity by modifying key proteins including α-amino-3-hydroxy-5-methyl-4-isoxazolepropionic acid (AMPA) receptors (1). Accumulating evidence suggests that small ubiquitin-like modifier (SUMO) conjugation (SUMOylation), an evolutionarily conserved post-translational modification, regulates a wide range of neuronal function, and is involved in learning and memory processes as well as neurogenerative diseases (2–11).

SUMOylation can affect the stability, activity, and localization of target proteins, and modulate their interactions with other proteins (3). Three SUMOs – SUMO1, SUMO2, and SUMO3 – are widely expressed in mammalian cells. SUMO1 shares approximately 50% homology with SUMO2/3, while SUMO2 and SUMO3 are almost identical and indistinguishable by available antibodies, and therefore are usually termed SUMO2/3. Importantly, SUMO2 is the predominant SUMO in mice (12). Similar to ubiquitin conjugation, SUMOylation occurs via the sequential actions of the SUMO E1 activating enzyme SAE1/2, the sole E2 conjugating enzyme Ubc9, and, depending upon the target protein, SUMO E3 ligases.

Many SUMOylation targets are proteins capable of modulating neuronal activity (3). These SUMO targets include transcription factors, ion channels, trafficking transport proteins, signaling kinases, and various synaptic proteins. Although conflicting findings have been reported on neuronal SUMOylation (3, 13), many studies – predominantly *in vitro* – suggest that SUMOylation can regulate neuronal function and synaptic plasticity. Consequently, a few studies have reported that cognitive processes are impacted by SUMOylation *in vivo*. For example, it has been suggested that SUMOylation of activity-regulated cytoskeleton-associated protein (Arc) contributes to synaptic plasticity (long-term potentiation, LTP) in dentate granule cells in the hippocampus (14). Notably, the Lee group has identified several

neuronal substrates of SUMOylation including STAT1, MeCP2, and CREB, and interestingly, they showed that a transient increase in SUMOylation of any of these proteins can critically affect memory processes (6–8). Together, these findings suggest that a dynamic net change in SUMOylation – that affects many neural proteins, rather than SUMOylation of only a few specific neuronal proteins – is a key regulator of cognitive function. In support of this notion, unlike ubiquitination or phosphorylation that exploits hundreds of ligases or kinases to control substrate specificity, the SUMOylation process relies on a sole E2 enzyme Ubc9 and a few E3 ligases; in many cases, E3 ligases are not even required for SUMOylation (15). Thus, substrate selection for SUMOylation is believed to be loosely regulated, further emphasizing the importance of global modulation of SUMOylation.

Indeed, simultaneous knockdown of SUMO1–3 expression in neurons causes impairment in both episodic and fear memories (2). Consistent with this finding, overexpression of a dominant negative form of the SUMO-conjugating enzyme Ubc9 results in impaired synaptic plasticity and cognition (9). However, the relative roles of the individual SUMOs in cognitive processes remain to be clarified. In particular, compared to SUMO1, SUMO2 has been rarely studied with respect to its role in neuronal functions – despite the fact that SUMO2 is the predominant SUMO in the mouse brain and global deletion of *Sumo2* is embryonically lethal (12). In the current study, we have generated a new conditional knockout mouse line in which *Sumo2* was deleted predominantly in forebrain neurons. These conditional *Sumo2* knockout mice were then subjected to a series of tests for cognitive function. Finally, changes in gene expression, neuronal morphology, and synaptic plasticity were assessed.

Materials and Methods

The protocols for all experiments were approved by the Duke University Institutional Animal Care and Use Committee.

Generation of conditional SUMO2 knockout mice

The targeting strategy to generate conditional Sumo2 knockout mice is illustrated in Figure 1A. Of note, the nomenclature for SUMO2 used here is in accordance with the NCBI database - protein entry number P61957. The BAC clone bMQ457C17, which contains the *Sumo2* genomic sequence, was identified from a 129Sv mouse genomic library (Source BioScience, Nottingham, UK) and used to retrieve the homologous arms. A targeting vector was constructed in which a flox site was placed into the third intron next to FLP sites that bounded the neomycin cassette (NEO; Fig. 1A). This cassette was adjacent to exon 4, which was followed by a flox site in intron 4. Approximately 8 kb downstream from this flox site was a thymidine kinase cassette (TK). Following verification by restriction analysis and partial sequencing, the targeting vector was submitted to the Duke Neurotransgenic Core Facility to generate chimeric mice. After germline transmission was confirmed, the FRT-flanked NEO cassette was removed by crossing the founder mice with transgenic mice expressing FLP recombinase under the control of a β-actin promoter to establish the conditional *Sumo2* line in which exon 4 of *Sumo2,* encoding the di-glycine motif essential

for functional SUMOylation, was floxed. The *Sumo2*$^{f/+}$ mice were backcrossed onto to a C57BL/6J background (The Jackson Laboratory, Bar Harbor, ME, USA) for more than 10 generations. To delete *Sumo2* in forebrain neurons, we crossed *Sumo2*$^{f/f}$ mice with Emx1$^{Cre/Cre}$ mice (JAX stock #005628; C57BL/6 background) to generate *Sumo2*$^{f/+}$;Emx1-Cre mice. These Cre mice were mated with homozygous *Sumo2*$^{f/f}$ mice to generate the experimental animals: *Sumo2*$^{f/f}$;Emx1-Cre (SUMO2-cKO) and *Sumo2*$^{f/f}$ or *Sumo2*$^{f/+}$ (controls). Genotyping was performed by PCR using tail genomic DNA with primers (F1 and R1) shown in Figure 1A (PCR products: ~ 620 bp for wild-type allele and ~710 bp for mutant allele). Genomic DNA from brain was used to confirm deletion of *Sumo2* exon 4. Standard PCR protocols were used. All primers are listed in Table S1.

Mice

Global *Sumo1* knockout (SUMO1-KO) mice were kindly provided by Dr. Kuehn (16). The global *Sumo3* knockout (SUMO3-KO) mice were generated previously in our lab (12), and generation of SUMO2-cKO mice and their controls is described above. All mice had been backcrossed onto a C57BL/6J background for more than 10 generations. Mice were housed 3–5/cage in a temperature- and humidity-controlled room under a 14:10 hour light:dark cycle with lights on from 0600 to 2000 hours. Access to food and water was provided *ad libitum*.

Behavioral studies

All behavioral studies were conducted in the Duke Mouse Behavioral and Neuroendocrine Analysis Core Facility. Behavioral tests were conducted with 3–6 month-old male and female control (*Sumo2*$^{f/f}$ or *Sumo2*$^{f/+}$) and SUMO2-cKO mice. Each experiment comprised 8–10 mice per group. Motor activity was assessed in the open field; anxiety-like behavior was evaluated in the open field and elevated zero maze; and tests for cognitive performance included analyses of sensory-motor gating (pre-attentive processing), spatial memory, episodic memory, memory load, and fear memory. To avoid possible associations between novel object recognition memory test and the spatial object displacement and memory load tests two separate sets of age- and sex-matched mice were used for testing. To neutralize any olfactory cues during object training and testing, the test-chambers and all objects were wiped before testing and in-between each mouse with LabSan256 CPQ (Sanitation Strategies, LLC, Holt, MI). All test-chambers and objects were dried with disposable towels. Additionally, investigators wore gloves during the studies and these were wiped in-between each mouse/test with LabSan 256 CPQ and dried with paper towels. As a control for the foot-shock in fear conditioning, the sensitivity to foot-shock was evaluated. All behavioral studies were conducted by researchers who were blinded to the mouse genotypes.

Open field activity: The open field (21 × 21 × 30 cm; Omnitech Inc., Columbus, OH, USA) was illuminated at 340 lux (17). Horizontal and vertical activities were monitored with a computer running Fusion software (Omnitech). To analyze spontaneous activity, mice were placed into the open field for 30 minutes, and motor activity was expressed as cumulative distance traveled, rearing (vertical beam-breaks), and activity in the center zone.

Elevated zero maze: This test has been described previously (17). Mice were tested under 40–60 lux illumination. Mice were placed individually into the closed area of the maze and given 5 minutes of free exploration. Videos were scored by using Observer XT11 (Noldus Information Technology, Leesburg, VA) and the data were expressed as the percent time in the open areas, latency to enter the open areas, and the frequency of closed-to-open-to-closed-area transitions.

Prepulse inhibition: Prepulse inhibition (PPI; San Diego Instruments, San Diego, CA) was evaluated as described (18). Testing comprised 3 trial types: null trials with only background noise (64 dB) and no additional auditory stimulus, pulse-alone trials with a 40 millisecond 120 dB white-noise startle stimulus, and prepulse-pulse trials in which the startle stimulus was preceded by 100 milliseconds with a 20 millisecond prepulse stimulus that was 4, 8, or 12 dB above the white-noise background (prepulse-pulse). Mice were placed into Plexiglas holders and acclimated for 10 minutes to the apparatus. Each test comprised 42 trials with 18 pulse alone, 6 null, and 18 prepulse-pulse trials comprised of 6 trials at each prepulse intensity. The test began with 6 pulse-alone trials followed by combinations of prepulse-pulse, pulse, and null trials, and ending with 6 pulse-alone trials. PPI was calculated as the ratio of the startle responses on prepulse-pulse trials to those on the startle-only trials, subtracted from 1 and expressed as a percentage [1 - (prepulse-pulse trials/pulse-alone trials)*100].

Short- and long-term episodic memory: Short-term memory (STM) and long-term memory (LTM) were assessed using the novel object recognition memory (NORM) test as described (2). Briefly, mice were acclimated to the empty chambers (25 × 25 × 14 cm; illuminated at 125 lux) 24 hours before testing. On day 1, animals were exposed to an identical pair of objects for 5 minutes. In the STM test (20 minutes after training), one of the familiar training objects was replaced with a novel object. Twenty-four hours after training, the remaining familiar training object was paired with a novel object for the LTM test. Behaviors were video-recorded with 3-point body detection (nose-center-tail) using Noldus Ethovision 11 (Leesburg, VA). Object recognition scores were calculated by subtracting the time spent with the novel object from the time spent with the familiar object, and dividing this difference by the total amount of time spent with both objects.

Spatial object memory: The test chamber consisted of a white Plexiglas arena (63 × 52 × 25 cm) illuminated at 125 lux. Three objects of similar size were placed in a line, with all objects 15 cm from the back wall, the first and third object positioned 15 cm from the walls at each end of the chamber, and all objects were separated by 25 cm from each other. Mice were habituated to the chamber for 5 minutes, were removed to their home-cages, and the objects were placed into the test arena. Training comprised three 5-minute exposures to the objects with a 15-minute inter-trial interval imposed between trials when the mouse was returned to its home-cage. After the final training trial, the third object was moved 20 cm straight-forward to a new location. Fifteen minutes after training, the mouse was tested for short-term spatial memory. All tests were video-taped and the videos were analyzed with Noldus Ethovision 11 software, as for episodic memory. The total duration of object contacts was determined as defined by the animal’s head oriented toward the object with the

nose positioned within 2 cm of the object. Recognition scores were calculated by subtracting the time spent with the displaced from the time spent with the two immobile objects, and dividing this number by the total time spent with all 3 objects. Positive scores signified recognition of the displaced object, negative scores indicated preferences for the immobile objects, and scores approaching 'zero' denoted preference for none of the objects.

Memory load: The same chamber used to test spatial memory was used here. Mice were subjected to 7 test trials; each was separated by a 10–15-second inter-trial interval (19). On each trial, a new object of similar size was added successively to the other objects. On trials 1–3, mice were allotted 3 minutes to explore the objects. On trials 4–5, they were given 4 minutes and on trials 6–7 they had 5 minutes. Testing commenced when the mouse was placed into the arena with the first object. At the end of this first trial, the mouse was removed to its home cage. The second object was added to the arena, and the mouse was returned to the test chamber. Mice were placed into the same location relative to the objects across all trials. On each trial the added object was termed the "target" object. All behaviors were video-taped and Noldus Ethovision 11 and nose-point tracking was used as for episodic memory. The duration of time spent with the target object and the mean time spent with the other objects was calculated from the tracking profiles for each trial. Memory load was determined on each trial by the success of the animal in selecting the target object over the other objects.

Fear conditioning: Fear conditioning responses were assessed as described (2). Briefly, mice were individually acclimated to the MedAssociates chambers (St. Albans, VT) for 2 minutes. The animal was then exposed to a 72-dB, 12-kHz tone for 30 seconds (conditioned stimulus; CS), that co-terminated with a 2-second 0.4-mA foot-shock (unconditioned stimulus; UCS). Thirty seconds after the CS-UCS pairing, the mouse was returned to its home cage. Twenty-four hours after conditioning, mice were returned to the same conditioning chamber for 5 minutes without exposure to the CS or UCS (context testing). After an additional 24 hours, mice were placed into a new environment for 2 minutes and this was followed by a 3-minute exposure to the CS alone without the UCS (cued testing). All tests were video-recorded and freezing behaviors were scored in real time using Cleversys Freeze Scan (Clever Sys Inc, Reston, VA).

Shock Threshold: Sensitivity to different intensities of scrambled foot shock was performed using a Med-Associates (St. Albans, VT) startle platform. Shock reactivity on each trial for each mouse was determined by the startle response of the animal following a given intensity of foot-shock. Mice were placed into a Plexiglas tube with a grid floor. Each grid was connected to a scrambler module by an electric harness (Med-Associates). This module produced varying intensities of scrambled foot-shock. Each test began with a 2 min acclimatization period. Subsequently, the animals were given 10 trials with 250 millisecond shocks separated by a 20–90 sec inter-trial interval. The intensities of the shocks were randomized across trials and consisted of 4 trials at 0 mA, and exposures to 0.1. 0.2, 0.3, 0.4, 0.5, and 0.6 mA scrambled shock. The first peak startle response by the animal was recorded within the first 1000 milliseconds after onset of the of shock stimulus. Peak startle reactivity was measured as arbitrary units (AU).

Preparation of total RNA

Total RNA was prepared from frozen hippocampal tissues. For quantitative reverse transcription PCR analysis, total RNA was extracted using TRIzol reagent (Invitrogen, Carlsbad, CA) without further purification. For RNA-Seq analysis, total RNA was treated with DNase I to digest residual genomic DNA, followed by column purification using the RNeasy MinElute Cleanup kit (Qiagen, Hilden, Germany), according to the manufacturer's instructions.

Quantitative reverse transcription PCR

Quantitative reverse transcription PCR (qRT-PCR) was performed as described (20). Briefly, using the SuperScript III First-Strand Synthesis System (ThermoFisher Scientific, Waltham, MA) and 500 ng of total RNA, cDNA samples were generated by reverse transcription. qRT-PCR was performed in a Lightcycler 2.0 (Roche Life Sciences, Indianapolis, IN). All primers used in this study are listed in Table S1.

RNA-Seq analysis

RNA-Seq analysis was performed in the Genomic Analysis and Bioinformatics Shared Resource at Duke University Medical Center. The quality and concentration of the RNA samples were assessed using a Bioanalyzer 2100 (Agilent Technologies, Santa Clara, CA) and Qubit 2.0 (ThermoFisher Scientific), respectively. Approximately 500 ng total RNA per sample was used for library construction. The NGS libraries were constructed using the KAPA Stranded mRNA-Seq Kit (Kapa BioSystems, Wilmington, MA). Poly(A) mRNAs were first captured using magnetic oligo-dT beads, fragmented using heat and magnesium, and reverse transcribed to produce double-strand cDNA (dscDNA). Illumina sequencing adapters were then ligated to the dscDNA fragments, and amplified to produce the final RNA-Seq library. Libraries were indexed using a single indexing approach, which permitted multiple libraries to be pooled and sequenced on the same sequencing lane using an Illumina HiSeq 4000 sequencing platform. Multiplexing 8 libraries per lane on an Illumina HiSeq 4000 flow cell yielded approximately 43 million 50-bp sequences per sample. Raw.bcl files generated by the sequencer were de-multiplexed and converted to fastq files using bcl2fastq2 v2.20. The raw data have been deposited in the GEO database with the accession number GSE108196.

RNA-Seq data were processed using the TrimGalore toolkit (version 0.4.1), which uses Cutadapt to trim low-quality bases and Illumina sequencing adapters from the 3' end of the reads. Only reads that were 20 nt or longer after trimming were reserved for further analysis. Reads were mapped to the GRCm38v68 version of the mouse genome and transcriptome using the STAR (version 2.5.0c) RNA-Seq alignment tool (21, 22). Reads were reserved for subsequent analysis if they mapped to a single genomic location. Gene counts were compiled using the HTSeq tool (version 0.6.1). Only genes that had at least 10 reads in any given library were used in the subsequent analysis. Normalization and differential expression were performed using the DESeq2 Bioconductor package (version 1.14.1) with the R (version 3.3.1) statistical programming environment (23). The false discovery rate (shown as p_{adj}) was calculated to control for multiple hypothesis testing. Due to a number of pseudo-

genes with > 98% similarity to the *Sumo2* gene, we re-aligned the reads with the STAR alignment algorithm, allowing reads to map up to 10 genomic locations.

Preparation of protein samples

Brain tissue samples were solubilized in our standard 2% SDS lysis buffer by sonication (24), except for enriched synaptic protein samples, which were prepared as follows. Synaptosomal fractions were enriched using the Syn-PER Synaptic Protein Extraction Reagent (ThermoFisher Scientific, Waltham, MA), according to the manufacturer's instructions. Briefly, protease and phosphatase inhibitors were added to the Syn-PER reagent immediately before use. Hippocampal samples (~ 50 mg) were homogenized in 500 μL with Syn-PER Reagent on ice. A 100-μL aliquot of total homogenate was reserved. The remaining 400 μL of total homogenate was centrifuged at 1200 × *g* for 10 minutes at 4°C. The supernatant was collected and centrifuged at 15,000 × *g* for 20 minutes at 4°C. This supernatant (cytosol fraction) was collected for Western blotting. The final synaptosome pellet was suspended in 100 μL Syn-PER reagent, and analyzed by Western blotting.

Western blotting

Western blot analysis was performed using our standard protocol (20). Protein samples were separated on 4%−15% Bis-Tris gels (Bio-Rad, Hercules, CA), and the proteins were transferred to PVDF membranes. After blocking with TBST (5% non-fat dry milk or 5% BSA), the PVDF membranes were incubated with the primary antibody overnight at 4°C. After incubating with the secondary antibody for 1 hour at room temperature, membranes were exposed to the ECL substrate solution (GE Healthcare Bio-Sciences, Pittsburgh, PA), and the proteins were detected using chemiluminescence. β-actin served as loading control. ImageJ software (NIH, Bethesda, MD) was used to quantify Western blots. All primary antibodies used in this study are listed in Table S1.

Histology and immunohistochemistry analysis

Mice were deeply anesthetized with isoflurane and transcardially perfused with saline, followed by 4% paraformaldehyde in saline. For Nissl staining, paraffin-embedded brain sections (5 μm) were de-paraffinized and rehydrated. Brain sections were stained with a 0.1% cresyl violet solution for 15 minutes, washed, dehydrated, and mounted. Images were taken using an Axio observer Z1 microscope (Carl Zeiss Microscopy LLC, Thornwood, NJ). Images at higher magnification were captured from hippocampal CA1 regions, and Image J software was used to count cell numbers. Five sections from each of 2 animals per group were used for histologic assessment. We counted the cells in a given area, and calculated the cell number per field (80000 μm^2).

Immunohistochemistry was performed as described (24). Briefly, immunofluorescence staining was performed on frozen sections (25 μm) using a free-floating staining method. The primary antibodies used in this study are listed in Table S1. Confocal images were generated using a Leica SP5 confocal microscope (Leica Microsystems, Buffalo Grove, IL). Whole-section images were generated by stitching multiple images together using a Zeiss Axio Imager Z2 motorized fluorescence microscope (Carl Zeiss Microscopy).

Dendritic spine density

To analyze dendritic spine density, Golgi staining was performed using the FD Rapid GolgiStain kit (FD NeuroTechnologies, Columbia, MD), according to the manufacturer's instructions (2). Briefly, mouse brains were quickly harvested and immersed in the impregnation solution for 2 weeks. Brains were then transferred to Solution C. Three days later, brains were frozen at −80°C, and brain sections (100 μm) were obtained using a cryostat. Randomly selected images of dendrites within the area of the CA1 *stratum radiatum* were analyzed using ImageJ software (NIH). The numbers of spines on each dendrite were counted, and these numbers were divided by the length of the dendrite. In total, 40–50 neurons per animal (n = 3 per group) were analyzed.

Transient brain ischemia surgeries

To induce ischemia in all brain regions including hippocampus and amygdala, our cardiac arrest and cardiopulmonary resuscitation (CA/CPR) mouse model was used (20). Briefly, mice were anesthetized with 5% isoflurane and were endotracheally intubated. Anesthesia was maintained with 1.5% isoflurane before CA induction. The electrocardiogram (EKG) was continuously monitored. After drawing 0.3 mL of blood from the jugular vein, 30 μL of 0.5 M KCl was infused to induce asystole, as verified by EKG and an absence of spontaneous respiration. Upon CA onset, lung ventilation ceased, and blood was re-infused 3 minutes later. After 8 minutes of CA, cardiopulmonary resuscitation was performed by epinephrine infusion and chest compressions. One hour later, animals were perfused and fixed for immunohistochemistry.

Transient forebrain ischemia was performed as described previously with minor modifications (24). Briefly, mice were anesthetized with 5% isoflurane. After endotracheal intubation, mice were mechanically ventilated under 1.5% isoflurane during surgery. Transient forebrain ischemia was induced by occluding both common carotid arteries for 10 minutes. Sham-operated mice underwent the same procedures except for occlusion. After 1 hour of reperfusion, animals were euthanized, and hippocampal samples were quickly dissected on ice, snap-frozen in liquid nitrogen, and stored at −80 °C until use for Western blotting.

Electrophysiology

Slice preparation: Acute hippocampal slices were prepared from mice (2–3 months old). Mice were deeply anesthetized with isoflurane and decapitated. Brains were rapidly removed and placed into ice-cold artificial cerebrospinal fluid (ACSF; pH 7.4) containing (in mM): 124 NaCl, 3 KCl, 1.25 NaH_2PO_4, 24 $NaHCO_3$, 2 $CaCl_2$, 2 $MgSO_4$, and 10 dextrose, and aerated with 95% O_2/5% CO_2. Coronal hippocampal slices (400 μm) were prepared using a Vibratome 1000 plus (Leica Microsystems, Buffalo Grove, IL). Slices were submerged ~5 mm in an oxygenated chamber and allowed to recover for 1 hour at room temperature. Slices were then incubated at 32°C (≥ 1 hour). For electrophysiologic recordings, slices were transferred to an interface slice chamber (flow rate for ACSF: 1.5 mL/min at 34°C).

Electrophysiology: The Schaffer collateral/commissural pathway was stimulated with a bipolar stimulating electrode inserted into the *stratum radiatum* of the hippocampal CA1 region. Stimulation was performed using single pulses (100 μs, 50–150 μA) delivered every 30 seconds. Extracellular glass microelectrodes (3–7 MΩ) filled with 0.2 mol/L NaCl were placed into the CA1 *stratum radiatum* to record evoked axonal fiber volley potentials (FV) and field excitatory postsynaptic potentials (fEPSP) using a Multiclamp 700B amplifier and pClamp digitizing software (Molecular Devices, San Jose, CA). The FV amplitudes and fEPSP slope and amplitudes were measured using Clampfit. Paired-pulse responses were monitored at various stimulus intervals (10, 20, 50, 100, 200, 500, and 1000 milliseconds). Ten trials were conducted for each stimulus frequency, and recordings were averaged over the trials. The facilitation ratio was calculated as the fEPSP-2/fEPSP-1 amplitude. Input/output curves for fEPSPs were generated for each slice by gradually increasing the stimulus intensity. The fEPSP initial slope was plotted against the FV amplitude to assess changes in basal synaptic transmission between genotypes. For LTP experiments the stimulus current was adjusted to evoke a fEPSP of 40% of the maximum response. After at least 20 minutes of baseline recording, LTP was induced by delivering two trains (1 second each) of stimuli at 100 Hz at 60 seconds interval. The initial maximum slope of the fEPSP was measured over a 0.5-ms time frame for all recordings in each slice and normalized to a 10-minute baseline immediately preceding the initial high-frequency stimulation to induce long-term potentiation (LTP). When necessary, we compensated for the spontaneous upward drift of the baseline by estimating the slope for each individual slice.

Statistical analyses

All data are presented as means ± SEM. Statistical analyses of the behavioral studies were performed using SPSS Statistical Analyses software version 25 (IBM Inc, Chicago, IL). Student's *t*-tests were used to analyze effects between 2 groups, and repeated-measures analysis of variance (RMANOVA) was used to analyze multiple measures on the same behavioral response within a single test. RMANOVA within-subject effects were designated for the percent inhibition in PPI across 3 different prepulse intensities; object preferences and time with objects in NORM, object displacement, and memory load; across shock intensities in shock threshold; and several time-points for conditioned fear and associated locomotor activity. Genotype was designated as the between-subjects effect. *Post hoc* analyses were performed with Bonferroni-corrected pairwise comparisons. Analysis of covariance (ANCOVA) was used to determine whether any association existed between immobility and locomotion in the fear conditioning experiment. A weighted least squares regression was used, where genotype effects for immobility were weighted by distance traveled by the respective animals. Electrophysiologic studies and other data, including Western blotting, qPCR, cell number, and spine density, were analyzed using Prism 8 software (GraphPad Software Inc, LaJolla, CA). For electrophysiologic studies, we tested 2–4 slices/mouse. At least 4 mice were used in each experimental group, and we considered each slice as an individual sample. Statistical differences were assessed using 2-way RMANOVA followed by Bonferroni's *post-hoc* analyses to assess significant differences between genotypes across time, stimulation intensity, or stimulation interval. Comparisons of 2 groups were analyzed with two-tailed unpaired Student *t*-test. A $p<0.05$ was considered statistically significant.

Results

Generation and characterization of *Sumo2* conditional knockout mice

To evaluate the role of specific SUMO conjugation in cognitive processes in detail, mutant mice in which a single SUMO was deleted were required. Since global deletion of *Sumo2* is lethal in mouse embryos (12), we generated a new conditional knockout mouse line *Sumo2*$^{f/f}$ in which exon 4 of the *Sumo2* gene was floxed (Fig. 1A). This exon is essential for functional SUMOylation because it encodes the di-glycine (GG) motif that is required to conjugate SUMO2 to lysine residues of target proteins. To delete *Sumo2* in forebrain excitatory neurons, we crossed *Sumo2*$^{f/f}$ mice with Emx1$^{Cre/Cre}$ mice to generate *Sumo2*$^{f/f}$;Emx1-Cre (ie, SUMO2-cKO) mice. In the following experiments, *Sumo2*$^{f/f}$ or *Sumo2*$^{f/+}$ littermates were used as controls for SUMO2-cKO mice. PCR analyses of brain DNA samples confirmed deletion of *Sumo2* exon 4 in the SUMO2-cKO mouse brain (Fig. 1B). We compared expression levels of 3 SUMOs in the hippocampus between control and knockout mice by qRT-PCR analysis (Fig. 1C). As expected, a dramatic reduction in *Sumo2* mRNA levels was found in SUMO2-cKO mice. Interestingly, in SUMO2-cKO mice, hippocampal *Sumo3* mRNA levels were significantly increased by approximately 1.64-fold compared to controls, whereas *Sumo1* mRNA levels were unchanged (Fig. 1C). This result suggests that *Sumo3* mRNA abundance is enhanced, possibly to compensate for the loss of *Sumo2*. Of note, there was no difference in expression of *Sumo1–3* in the brain between wild-type and *Sumo2*$^{f/f}$ mice (Fig. S1A). An analysis of the genotypic distribution in progeny revealed normal Mendelian ratios for the pups from SUMO2-cKO litters (Table S2). Moreover, SUMO2-cKO mice exhibited no overt anomalies and had a normal brain structure as characterized by Nissl staining (Fig. S1B).

Under physiologic conditions, SUMO2/3 are found primarily as free SUMO proteins. We therefore examined protein levels of unconjugated SUMO2/3 in 3 different brain regions of SUMO2-cKO mice. As expected, SUMO2/3 was markedly reduced in forebrain samples (cortex and hippocampus) of SUMO2-cKO relative to control mice, but not in cerebellum (internal control; Fig. S1C). This dramatic decrease further confirmed our previous finding that SUMO2 is the predominantly expressed SUMO in the mouse brain (12). Next, to better visualize SUMO2/3 signals in the brain, we subjected mice to transient global brain ischemia because ischemia/reperfusion greatly increases the levels and nuclear accumulation of SUMO2/3-conjugated proteins (24). After 8 minutes of global brain ischemia and 1 hour reperfusion, brains were harvested for immunohistochemistry. The SUMO2/3 immunostaining signal was notably concentrated in the nuclei of CA1 hippocampal and amygdala neurons in wild-type (WT) and SUMO1-KO mice (Fig. 1D). By contrast, the SUMO2/3 signal was very low in CA1 neurons and it was clearly reduced in amygdala neurons in SUMO2-cKO mice (Fig. 1D and Fig. S1D).

Finally, to evaluate the effect of SUMO deficiencies on SUMOylation dynamics, we subjected SUMO mutant mice to ischemia/reperfusion stress, and analyzed changes in hippocampal SUMOylation (Fig. 1E). As expected, ischemia-activated SUMO1 conjugation was only affected in SUMO1-KO mice. Similarly, SUMO2/3 conjugation was markedly reduced only in SUMO2-cKO mice, while deficiencies in SUMO2 and SUMO3 exerted no

obvious effects on SUMO1 conjugation. Taken together, the dynamics of the SUMO2/3 conjugation response was severely impaired in the SUMO2-cKO brain.

Loss of SUMO2 in the brain is detrimental to cognitive functions.

After having verified and characterized SUMO2-cKO mice, we examined the effects of *Sumo2* deletion on various neurobehavioral functions. Of note, since no sex differences were observed on any of the behavioral tests, this variable was collapsed across the genotypes. SUMO2 mutant mice were evaluated initially for spontaneous motor activity and anxiety-like behavior. While rearing activities were not different between genotypes, there was a weak trend for locomotion to be higher in the SUMO2-cKO than control mice (Fig. 2A). This trend was driven entirely by two SUMO2-cKO animals, while the distribution of locomotor activities for all other mutants was virtually identical to that of the controls. In tests for anxiety-like behaviors, the open field (center distance traveled) and elevated zero maze tests failed to discern any significant genotype effects (Fig. 2). In preparation for the cognitive tests, prepulse inhibition (PPI) was evaluated; no significant genotype differences were noted for null activity, startle activity, or PPI (Fig. S2A). Collectively, these data indicate that motor performance, anxiety status, and pre-attentive processes are normal in SUMO2-cKO mice.

Next, to assess a specific role of SUMO2 on cognitive performance, we subjected the mutant mice to a series of memory tasks. Results from the NORM test indicated that SUMO2-cKO mice were severely impaired in both short-term memory (STM; $p<0.001$) and long-term memory (LTM; $p<0.001$) relative to their respective controls (Fig. 3A). These striking genotype differences could not be attributed to a failure to interact with the objects since the time spent exploring objects was similar between the genotypes at training and testing (Table S3A).

As a further assessment, we conducted a test for spatial object memory, which is proposed to depend primarily on hippocampal function (25). While control mice demonstrated a strong preference for the displaced object, performance of the SUMO2-cKO mice ($p<0.001$) was significantly inferior to the respective control animals (Fig. 3B), indicating an impairment in spatial memory. Of note, no genotype differences were observed with respect to their interactions with the objects at training or testing (Table S3B).

In the final object test, memory load was examined. Here, 7 different objects were presented in succession, and the mouse had to identify the novel object (Fig. 3C). Control mice had no difficulties in recognizing the target or novel object when presented with as many as 6 additional objects. By comparison, preference for the target object was significantly impaired in the SUMO2-cKO relative to controls at each memory load examined; 2 ($p=0.018$), 3 ($p=0.052$), 4 ($p=0.026$), 5 ($p=0.005$), 6 ($p=0.027$), and 7 ($p=0.002$) objects. Of note, all genotypes interacted with the objects to similar extents (Table S3C). Collectively, the results from these object tests demonstrated that SUMO2-cKO mice were severely impaired in episodic and spatial memory and had difficulties retaining the items in memory over short durations.

Lastly, to assess emotional memory we conducted fear conditioning tests (Fig. 3D). No genotype differences were observed at each stage of conditioning (Fig. 3D, *left*). Following conditioning, all mice were tested for contextual fear 24 hours later. Here, SUMO2-cKO mice were deficient relative to control mice ($p = 0.004$; Fig. 3D, *middle*). Twenty-four hours after examining contextual fear, mice were tested for cued fear. The magnitude of freezing behaviors or immobility was higher during the pre-CS interval in control than in SUMO2-cKO mice ($p = 0.024$; Fig. 3D, *right*). When the CS was presented, immobility was less pronounced in the mutant than in the control mice ($p = 0.022$). These findings are not due to differential abilities of the genotype to respond to foot-shock since their responses are comparable to different levels of shock (Fig. S2B). Moreover, in light of the open field data, more data analyses were performed and indicated that the weak trend for locomotion to be higher in SUMO2-cKO than control mice was not a confounding factor in the deficiency of SUMO2-cKO mice in both contextual and fear memory (please also see the supplemental results, Fig. S3, and Table S4).

SUMO2-cKO mice have normal brain morphologies

As a first step toward dissecting mechanisms associated with the behavioral phenotypes found in SUMO2-cKO mice, we compared the number of neurons in the CA1 hippocampal field and found no genotype differences (Fig. 4A). Since SUMOylation modulates spinogenesis (26, 27) and a decrease in dendritic spine numbers can reflect memory dysfunction, we quantified spine densities on pyramidal neurons in the CA1 hippocampal region and found no significant differences among groups (Fig. 4B). Together, these data suggest that the behavioral alterations are not likely attributed to differences in neural morphology between genotypes.

Global gene expression is moderately modulated in the SUMO2-cKO hippocampus

Since SUMO2 is the predominant SUMO in mice (12) and many SUMO targets are transcription factors or other nuclear proteins that modulate gene expression (3), we then hypothesized that deletion of *Sumo2* may constitutively alter expression of a subset of genes related to memory functions. Since memory-related molecular mechanisms have been extensively studied in hippocampus, RNA-Seq analyses were performed on hippocampal samples from SUMO2-cKO and control mice. Based upon our selection criteria (fold change ≥ 1.5 and a false discovery rate-corrected p-value, $p_{adj} \leq 0.05$), only 58 genes were differentially regulated (49 upregulated and 9 downregulated) in SUMO2-cKO vs control mice (Fig. 5A and Table S5). A qRT-PCR analyses of 5 of the 58 genes validated our RNA-Seq data (Fig. 5B). These findings agree with our previous results that under physiologic conditions, silencing SUMO expression primarily upregulates gene expression in the brain (28). Overall, our findings indicate that deficiency of SUMO2 in hippocampus moderately affects global gene expression.

Among the 58 genes that were differentially regulated, *Sumo3* was upregulated 1.62-fold in SUMO2-cKO vs control mice (Table S5), similar to our qRT-PCR result (Fig. 1C). To our surprise, we did not identify *Sumo2* as a differentially expressed gene in our initial analysis. Further analyses indicated that, due to the presence of multiple pseudo-genes with almost identical sequences to the *Sumo2* cDNA and our 50 bp single-end sequencing strategy, most

of the reads that should have mapped to *Sumo2* were filtered-out. Indeed, targeted analysis of the *Sumo2* gene, which allows reads to map to multiple locations, showed a substantial decrease in the number of reads in SUMO2-cKO relative to control mice (Fig. 5C). Finally, a pathway analysis of the 58 genes failed to identify any memory-related pathway. Hence, our RNA-Seq data suggest that constitutive changes in gene expression produced by *Sumo2* deletion unlikely played a major role in the behavioral phenotype in SUMO2-cKO mice.

Synaptic protein levels were not significantly different in SUMO2-cKO vs control mice

Since synaptic plasticity is a key cellular mechanism for memory processes (1, 29), and post-translational modifications can affect synaptic plasticity by dynamically modulating synaptic proteins, we examined both AMPA and N-methyl D-aspartate (NMDA) receptors. We quantified the protein levels of the AMPA receptor (GluR1–4) and NMDA receptor (NR1, NR2A, and NR2B) subunits in whole hippocampal tissue lysates from SUMO2-cKO and control mice. We found no significant genotype differences in expression of the protein levels for these receptor subunits (Fig. 6A,B). Since these receptors constantly undergo activity-dependent translocation and changes in subunit composition at synapses, we prepared synaptosome fractions from the hippocampus. As expected, the post-synaptic marker PSD95 and the pre-synaptic marker synaptophysin were enriched in our synaptosome fraction (Fig. S4). Although there was a trend towards reduced levels of GluR2–4, NR2A, and PSD-95 proteins in SUMO2-cKO compared to control mice, this effect was not statistically significant (Fig. 6C,D). These data demonstrate that deletion of *Sumo2* has no significant effect on expression of AMPA and NMDA receptor subunits as well as synaptophysin and PSD-95 under non-stimulated conditions.

Hippocampal LTP was impaired in SUMO2-cKO mice

Finally, we examined the effects of deletion of *Sumo2* on activity-dependent synaptic plasticity by assessing hippocampal LTP. To estimate basal synaptic transmission at CA3-CA1 synapses in the hippocampus, the Schaffer collaterals were stimulated at varying stimulation intensity and input-output (I/O) curves were analyzed for pre-synaptic axonal fiber volley (FV) amplitude and field excitatory postsynaptic potentials (fEPSP).

SUMO2-cKO mice demonstrated a significant change in basal synaptic transmission according to the fEPSP and pre-synaptic FV I/O relationship (Fig. 7A). The ratio of fEPSP slope to presynaptic FV was significantly smaller in SUMO2-cKO (Fig. 7B). Although the amplitude of the presynaptic FV amplitude was not different between SUMO2-cKO mice and control littermates (Fig. 7C), we observed a decrease of the fEPSP slopes in SUMO2-cKO slices, with a significant reduction of the mean regression slope values of the I/O curve (Fig. 7D,E). These results indicate an alteration in synaptic strength rather than fiber excitability in SUMO2-cKO animals. We next examined potential genotype differences for pre-synaptic release probability with paired pulse facilitation. With this measure of short-term plasticity, we found no significant difference between SUMO2-cKO and their control littermates (Fig. 7F,G). However, the mean increase in the fEPSP slope for LTP at 60 minutes was significantly smaller in SUMO2-cKO than in control slices (132.7 ± 7.4% vs 182.9 ± 8.3%, at 55–60 minutes post stimulation; $p < 0.0005$) (Fig. 7H, I). Taken together, these findings reveal that LTP was significantly impaired in SUMO2-cKO mouse brains.

Discussion

In the present study, we conducted the first *in vivo* experiments to investigate the specific role of SUMO2 in cognitive performance. Since *Sumo2*$^{-/-}$ embryos die at approximately embryonic day 10.5 (12), we generated new SUMO2 conditional knockout (SUMO2-cKO) mice by deleting *Sumo2* predominantly in the forebrain neurons. These SUMO2-cKO mice were born at the expected Mendelian ratios, were healthy, and showed no overt phenotype. Because Emx1$^{Cre/Cre}$ mice were used to conditionally delete *Sumo2* in forebrain neurons, Emx1 expression is active as early as embryonic day 10 (30) and because the SUMO2-cKO mouse brain morphology appeared normal, our data suggest that SUMO2 is not essential for neuronal development and neural maintenance in the forebrain. Additionally, since SUMO2 is the predominant SUMO and is indispensable for embryonic development, the new *Sumo2*$^{f/f}$ mouse line is a critical addition to the genetic tools for SUMO research that currently include the *Sumo1*$^{-/-}$, *Sumo2*$^{+/-}$, *Sumo3*$^{-/-}$, CAG-SUMO, His_6-HA-SUMO1, and SUMO-KD mouse lines (2, 12, 16, 24, 31).

We have conducted a comprehensive behavioral phenotyping screen to assess potential neurobehavioral abnormalities in SUMO2-cKO mice. Initial experiments revealed that spontaneous locomotor and rearing activities, as well as pre-attentive functions were normal in these mutants. Strikingly, in the NORM test, SUMO2-cKO mice were remarkably impaired in both STM and LTM compared to controls. We also found that SUMO2-cKO mice were impaired in the spatial object displacement task, the test for memory load, and in contextual and cued fear conditioning. These data clearly indicate that SUMO2 is critically involved in cognitive processes.

Our results further show that SUMO2 deficiency in the brain does not lead to permanent changes in structural and/or protein levels directly involved in cognitive performance. Thus, it is plausible to propose that the behavioral phenotypes observed in the SUMO2 mutant mice are due most likely to impairment in dynamic SUMOylation processes associated with synaptic plasticity. However, due to the rapid and reversible nature of SUMOylation, it is difficult to definitively demonstrate how SUMOylation is temporally and spatially modulated during various phases of cognition. One possible way to address this issue may be to perform comprehensive unbiased SUMO proteomics studies at each stage of the cognitive tests using our SUMO2 transgenic mice (24). However, even this approach may be unsatisfactory when considering the rapid rate of active SUMOylation/de-SUMOylation cycling, and the extremely low abundance of the individual SUMO-conjugated neuronal proteins that may be associated with synaptic plasticity. Clearly, future studies are warranted to further dissect the underlying dynamic, molecular mechanisms of SUMO2 deficiency as it relates to aberrant cognitive processes.

Our behavioral studies clearly indicate a deficit in hippocampus-dependent memory processes. Synaptic plasticity is essential for memory function and hippocampal LTP is one of the most widely used cellular models for investigating mechanisms that underlie synaptic plasticity (1, 29). Using hippocampal slices, we found that LTP induced by high frequency stimulation was decreased significantly in SUMO2-cKO relative to control mice, indicating a significant impairment of post-synaptic mechanisms that support long-lasting synaptic

plasticity (32). Interestingly, short-term plasticity, a measure of pre-synaptic calcium and post-synaptic inhibition (33), was unchanged between SUMO2-cKO and control slices. However, the significant decrease in basal synaptic transmission in SUMO2-cKO mice indicates reduced synaptic strength. As demonstrated by the I/O relationship analysis, this reduction was not related to changes in pre-synaptic axonal excitability. Though it is possible that pre-synaptic release mechanisms are altered in the SUMO2-cKO mice, neither the synaptosome data nor the paired-pulse data indicate this is the case, indicating the most likely cause of the reduced synaptic strength is post-synaptic alterations (34). Of note, involvement of SUMOylation in synaptic plasticity has been studied previously; however, these studies were performed predominantly in primary neuronal cultures and in hippocampal slices, and most of these studies focused on SUMO1 conjugation (14, 35–37). For example, it has been shown that Arc and GluK2 can only be conjugated by SUMO1, but not by SUMO2/3 in the brain (35, 37). By comparison, in the present study, we found that selective deletion of *Sumo2* in an excitatory neuronal population is sufficient to produce severe impairments in a variety of cognitive processes and in hippocampal LTP. Thus, these results indicate that the critical proteins/processes that exert essential roles in synaptic plasticity and that are modulated by SUMO2/3, but not by SUMO1 conjugation, have not yet been identified.

There is evidence that LTP is a cellular mechanism involved with memory, suggested by occlusion interactions between specific memory formation and LTP induction (38). There are at least two separate phases of LTP: induction and expression (39). In CA1 hippocampus, induction of LTP involves presynaptic glutamate release resulting in depolarization of postsynaptic neurons through the high frequency trains. The NMDA receptors (NMDARs) on postsynaptic neurons are particularly important for LTP expression, since antagonism of NMDARs with AP5 blocks the induction of LTP and spatial learning in the water maze (40). Conversely, prior saturation of LTP impairs the encoding of new memory (41, 42). LTP consists of different forms that are independent and dependent upon de novo protein synthesis (43). For instance, LTPa lasts for several hours and, depending upon the protocol, does not require protein synthesis. By comparison, LTPb lasts over many hours and is dependent upon protein synthesis. The SUMO2-cKO mice were deficient in both STM (NORM, spatial object memory, and memory load) as well as LTM (NORM and contextual/cued fear conditioning). The rapid decline in the fEPSP slope in hippocampus following the high frequency stimulation trains in the SUMO2-cKO suggests that induction of LTP is abnormal. The persistent reduction in hippocampal LTP over the initial 1 hour period in the SUMO2-cKO mice is consistent with the STM deficits in the SUMO2- cKO mice. However, these mutants are also partially deficient in contextual and cued fear conditioning, indicating a wide array of memory processes are affected by the SUMO2-cKO. Future work is needed to disentangle these underlying molecular and cellular processes.

There may be some limitations to our studies. First, in the experiments we used littermate *Sumo2*$^{f/f}$ or *Sumo2*$^{f/+}$ as control mice, based on our mating strategy. While we did not use Emx1-Cre mice as controls, they have been used extensively in neuroscience research and, to our knowledge, no behavioral abnormity has been reported in this mouse line (44). Hence, it is unlikely that the phenotype observed in our experiments is due to insertion of the Cre

transgene into the genome. Second, our RNA-Seq analysis likely did not reveal all genes that are differentially regulated in neurons between control and SUMO2-cKO mice, because whole hippocampal tissues were used. Finally, our current analysis focused primarily on neuronal proteins that are known to be related to synaptic activity. However, deletion of *Sumo2* in excitatory neurons may affect non-synaptic pathways that indirectly modulate synaptic plasticity and thereby, contribute to the cognitive defects. Indeed, unbiased proteomics studies have identified thousands of SUMOylation substrates and SUMOylation is believed to regulate almost all major signaling events (45). Future studies need to consider the possible involvement of non-synaptic mechanisms mediated by protein SUMOylation in neuronal functions.

In summary, this is the first study to investigate the role of individual SUMOs in cognitive processes and LTP using SUMO-specific knockout mice. Our results indicate that deletion of *Sumo2* leads to dysfunction in dynamic SUMOylation processes, resulting in impaired synaptic plasticity and cognitive dysfunction. Thus, protein conjugation by SUMO2 is critically involved in cognitive processes in mice. Further, since levels of global SUMOylation in the brain decrease with aging (9) and the capacity to induce SUMOylation after environment changes is reduced in the aged brain (20, 46), our findings suggest that inadequate SUMO conjugation responses may be related to cognitive decline observed in the elderly.

Supplementary Material

Refer to Web version on PubMed Central for supplementary material.

Acknowledgements:

We thank Dr. David Corcoran for his support in RNA-Seq data analysis, Dr. Donna Niedzwiecki for her advice in electrophysiology data analysis, Pei Miao and Qiang Chen for their excellent technical support, Christopher Means, Fiona A. Porkka, David Zhou, Autumn Q. Wetsel, and Laura-Jöelle Geschwindt for their assistance in the behavioral studies, and Kathy Gage for her excellent editorial contribution. Some of the equipment and software used in the behavioral experiments were purchased with a grant from the North Carolina Biotechnology Center. This study was supported by funds from the Department of Anesthesiology (Duke University Medical Center), American Heart Association grant 16GRNT30270003 (to WY), and NIH NS081299 (to WP).

Abbreviations:

SUMO	small ubiquitin-like modifier
AMPA	α-amino-3-hydroxy-5-methyl-4-isoxazolepropionic acid
NMDA	N-methyl D-aspartate
Arc	activity-regulated cytoskeleton-associated protein
LTP	long-term potentiation
WT	wild-type
KO	knockout
cKO	conditional knockout

PPI	prepulse inhibition
NORM	novel object recognition memory
STM	short-term memory
LTM	long-term memory
CS	conditioned stimulus
UCS	unconditioned stimulus
AU	arbitrary units
CA/CPR	cardiopulmonary resuscitation
ACSF	artificial cerebrospinal fluid
fEPSP	field excitatory postsynaptic potentials
I/O	input/output

References

1. Ho VM, Lee JA, and Martin KC (2011) The cell biology of synaptic plasticity. Science 334, 623–628 [PubMed: 22053042]
2. Wang L, Rodriguiz RM, Wetsel WC, Sheng H, Zhao S, Liu X, Paschen W, and Yang W (2014) Neuron-specific Sumo1–3 knockdown in mice impairs episodic and fear memories. J Psychiatr Neurosci 39, 259–266
3. Henley JM, Craig TJ, and Wilkinson KA (2014) Neuronal SUMOylation: mechanisms, physiology, and roles in neuronal dysfunction. Physiol Rev 94, 1249–1285 [PubMed: 25287864]
4. Matsuzaki S, Lee L, Knock E, Srikumar T, Sakurai M, Hazrati LN, Katayama T, Staniszewski A, Raught B, Arancio O, and Fraser PE (2015) SUMO1 Affects Synaptic Function, Spine Density and Memory. Sci Rep 5, 10730 [PubMed: 26022678]
5. Ripamonti S, Shomroni O, Rhee JS, Chowdhury K, Jahn O, Hellmann KP, Bonn S, Brose N, and Tirard M (2020) SUMOylation controls the neurodevelopmental function of the transcription factor Zbtb20. J Neurochem.
6. Tai DJ, Hsu WL, Liu YC, Ma YL, and Lee EH (2011) Novel role and mechanism of protein inhibitor of activated STAT1 in spatial learning. EMBO J 30, 205–220 [PubMed: 21102409]
7. Chen YC, Hsu WL, Ma YL, Tai DJ, and Lee EH (2014) CREB SUMOylation by the E3 ligase PIAS1 enhances spatial memory. J Neurosci 34, 9574–9589 [PubMed: 25031400]
8. Tai DJ, Liu YC, Hsu WL, Ma YL, Cheng SJ, Liu SY, and Lee EH (2016) MeCP2 SUMOylation rescues Mecp2-mutant-induced behavioural deficits in a mouse model of Rett syndrome. Nat Commun 7, 10552 [PubMed: 26842955]
9. Lee L, Dale E, Staniszewski A, Zhang H, Saeed F, Sakurai M, Fa M, Orozco I, Michelassi F, Akpan N, Lehrer H, and Arancio O (2014) Regulation of synaptic plasticity and cognition by SUMO in normal physiology and Alzheimer's disease. Sci Rep 4, 7190 [PubMed: 25448527]
10. Steffan JS, Agrawal N, Pallos J, Rockabrand E, Trotman LC, Slepko N, Illes K, Lukacsovich T, Zhu YZ, Cattaneo E, Pandolfi PP, Thompson LM, and Marsh JL (2004) SUMO modification of Huntingtin and Huntington's disease pathology. Science 304, 100–104 [PubMed: 15064418]
11. Grupe A, Abraham R, Li Y, Rowland C, Hollingworth P, Morgan A, Jehu L, Segurado R, Stone D, Schadt E, Karnoub M, Nowotny P, Tacey K, Catanese J, Sninsky J, Brayne C, Rubinsztein D, Gill M, Lawlor B, Lovestone S, Holmans P, O'Donovan M, Morris JC, Thal L, Goate A, Owen MJ, and Williams J (2007) Evidence for novel susceptibility genes for late-onset Alzheimer's disease

from a genome-wide association study of putative functional variants. Hum Mol Genet 16, 865–873 [PubMed: 17317784]

12. Wang L, Wansleeben C, Zhao S, Miao P, Paschen W, and Yang W (2014) SUMO2 is essential while SUMO3 is dispensable for mouse embryonic development. EMBO Rep 15, 878–885 [PubMed: 24891386]
13. Daniel JA, Cooper BH, Palvimo JJ, Zhang FP, Brose N, and Tirard M (2017) Analysis of SUMO1-conjugation at synapses. Elife 6, e26338. [PubMed: 28598330]
14. Nair RR, Patil S, Tiron A, Kanhema T, Panja D, Schiro L, Parobczak K, Wilczynski G, and Bramham CR (2017) Dynamic Arc SUMOylation and Selective Interaction with F-Actin-Binding Protein Drebrin A in LTP Consolidation In Vivo. Front Synaptic Neurosci 9, 8 [PubMed: 28553222]
15. Gareau JR, and Lima CD (2010) The SUMO pathway: emerging mechanisms that shape specificity, conjugation and recognition. Nat Rev Mol Cell Bio 11, 861–871 [PubMed: 21102611]
16. Evdokimov E, Sharma P, Lockett SJ, Lualdi M, and Kuehn MR (2008) Loss of SUMO1 in mice affects RanGAP1 localization and formation of PML nuclear bodies, but is not lethal as it can be compensated by SUMO2 or SUMO3. J Cell Sci 121, 4106–4113 [PubMed: 19033381]
17. Pogorelov VM, Rodriguiz RM, Insco ML, Caron MG, and Wetsel WC (2005) Novelty seeking and stereotypic activation of behavior in mice with disruption of the Dat1 gene. Neuropsychopharmacology 30, 1818–1831 [PubMed: 15856082]
18. Pogorelov VM, Rodriguiz RM, Cheng J, Huang M, Schmerberg CM, Meltzer HY, Roth BL, Kozikowski AP, and Wetsel WC (2017) 5-HT2C Agonists Modulate Schizophrenia-Like Behaviors in Mice. Neuropsychopharmacology 42, 2163–2177 [PubMed: 28294132]
19. Sannino S, Russo F, Torromino G, Pendolino V, Calabresi P, and De Leonibus E (2012) Role of the dorsal hippocampus in object memory load. Learn Mem 19, 211–218 [PubMed: 22523415]
20. Shen Y, Yan B, Zhao Q, Wang Z, Wu J, Ren J, Wang W, Yu S, Sheng H, Crowley SD, Ding F, Paschen W, and Yang W (2018) Aging Is Associated With Impaired Activation of Protein Homeostasis-Related Pathways After Cardiac Arrest in Mice. J Am Heart Assoc 7, e009634 [PubMed: 30371162]
21. Kersey PJ, Staines DM, Lawson D, Kulesha E, Derwent P, Humphrey JC, Hughes DS, Keenan S, Kerhornou A, Koscielny G, Langridge N, McDowall MD, Megy K, Maheswari U, Nuhn M, Paulini M, Pedro H, Toneva I, Wilson D, Yates A, and Birney E (2012) Ensembl Genomes: an integrative resource for genome-scale data from non-vertebrate species. Nucleic Acids Res 40, D91–97 [PubMed: 22067447]
22. Dobin A, Davis CA, Schlesinger F, Drenkow J, Zaleski C, Jha S, Batut P, Chaisson M, and Gingeras TR (2013) STAR: ultrafast universal RNA-seq aligner. Bioinformatics 29, 15–21 [PubMed: 23104886]
23. Huber W, Carey VJ, Gentleman R, Anders S, Carlson M, Carvalho BS, Bravo HC, Davis S, Gatto L, Girke T, Gottardo R, Hahne F, Hansen KD, Irizarry RA, Lawrence M, Love MI, MacDonald J, Obenchain V, Oles AK, Pages H, Reyes A, Shannon P, Smyth GK, Tenenbaum D, Waldron L, and Morgan M (2015) Orchestrating high-throughput genomic analysis with Bioconductor. Nat Methods 12, 115–121 [PubMed: 25633503]
24. Yang W, Sheng H, Thompson JW, Zhao S, Wang L, Miao P, Liu X, Moseley MA, and Paschen W (2014) Small ubiquitin-like modifier 3-modified proteome regulated by brain ischemia in novel small ubiquitin-like modifier transgenic mice: putative protective proteins/pathways. Stroke 45, 1115–1122 [PubMed: 24569813]
25. Vogel-Ciernia A, and Wood MA (2014) Examining object location and object recognition memory in mice. Curr Protoc Neurosci 69, 8 31 31–17 [PubMed: 25297693]
26. Shalizi A, Gaudilliere B, Yuan Z, Stegmuller J, Shirogane T, Ge Q, Tan Y, Schulman B, Harper JW, and Bonni A (2006) A calcium-regulated MEF2 sumoylation switch controls postsynaptic differentiation. Science 311, 1012–1017 [PubMed: 16484498]
27. Chao HW, Hong CJ, Huang TN, Lin YL, and Hsueh YP (2008) SUMOylation of the MAGUK protein CASK regulates dendritic spinogenesis. J Cell Biol 182, 141–155 [PubMed: 18606847]
28. Zhang L, Liu X, Sheng H, Liu S, Li Y, Zhao JQ, Warner DS, Paschen W, and Yang W (2017) Neuron-specific SUMO knockdown suppresses global gene expression response and worsens

functional outcome after transient forebrain ischemia in mice. Neuroscience 343, 190–212 [PubMed: 27919694]

29. Kandel ER, Dudai Y, and Mayford MR (2014) The molecular and systems biology of memory. Cell 157, 163–186 [PubMed: 24679534]
30. Simeone A, Acampora D, Gulisano M, Stornaiuolo A, and Boncinelli E (1992) Nested expression domains of four homeobox genes in developing rostral brain. Nature 358, 687–690 [PubMed: 1353865]
31. Tirard M, Hsiao HH, Nikolov M, Urlaub H, Melchior F, and Brose N (2012) In vivo localization and identification of SUMOylated proteins in the brain of His6-HA-SUMO1 knock-in mice. Proc Natl Acad Sci U S A 109, 21122–21127 [PubMed: 23213215]
32. Granger AJ, and Nicoll RA (2014) Expression mechanisms underlying long-term potentiation: a postsynaptic view, 10 years on. Philos Trans R Soc Lond B Biol Sci 369, 20130136 [PubMed: 24298139]
33. Bartley AF, and Dobrunz LE (2015) Short-term plasticity regulates the excitation/inhibition ratio and the temporal window for spike integration in CA1 pyramidal cells. Eur J Neurosci 41, 1402–1415 [PubMed: 25903384]
34. Jackman SL, Turecek J, Belinsky JE, and Regehr WG (2016) The calcium sensor synaptotagmin 7 is required for synaptic facilitation. Nature 529, 88-+ [PubMed: 26738595]
35. Craig TJ, Jaafari N, Petrovic MM, Jacobs SC, Rubin PP, Mellor JR, and Henley JM (2012) Homeostatic synaptic scaling is regulated by protein SUMOylation. J Biol Chem 287, 22781–22788 [PubMed: 22582390]
36. Chamberlain SE, Gonzalez-Gonzalez IM, Wilkinson KA, Konopacki FA, Kantamneni S, Henley JM, and Mellor JR (2012) SUMOylation and phosphorylation of GluK2 regulate kainate receptor trafficking and synaptic plasticity. Nat Neurosci 15, 845–852 [PubMed: 22522402]
37. Martin S, Nishimune A, Mellor JR, and Henley JM (2007) SUMOylation regulates kainate-receptor-mediated synaptic transmission. Nature 447, 321–325 [PubMed: 17486098]
38. Whitlock JR, Heynen AJ, Shuler MG, and Bear MF (2006) Learning induces long-term potentiation in the hippocampus. Science 313, 1093–1097 [PubMed: 16931756]
39. Nicoll RA (2017) A Brief History of Long-Term Potentiation. Neuron 93, 281–290 [PubMed: 28103477]
40. Morris RG, Anderson E, Lynch GS, and Baudry M (1986) Selective impairment of learning and blockade of long-term potentiation by an N-methyl-D-aspartate receptor antagonist, AP5. Nature 319, 774–776 [PubMed: 2869411]
41. Castro CA, Silbert LH, McNaughton BL, and Barnes CA (1989) Recovery of spatial learning deficits after decay of electrically induced synaptic enhancement in the hippocampus. Nature 342, 545–548 [PubMed: 2586626]
42. Moser EI, Krobert KA, Moser MB, and Morris RG (1998) Impaired spatial learning after saturation of long-term potentiation. Science 281, 2038–2042 [PubMed: 9748165]
43. Park P, Volianskis A, Sanderson TM, Bortolotto ZA, Jane DE, Zhuo M, Kaang BK, and Collingridge GL (2014) NMDA receptor-dependent long-term potentiation comprises a family of temporally overlapping forms of synaptic plasticity that are induced by different patterns of stimulation. Philos Trans R Soc Lond B Biol Sci 369, 20130131 [PubMed: 24298134]
44. Nakajima M, Gorlich A, and Heintz N (2014) Oxytocin modulates female sociosexual behavior through a specific class of prefrontal cortical interneurons. Cell 159, 295–305 [PubMed: 25303526]
45. Hendriks IA, and Vertegaal AC (2016) A comprehensive compilation of SUMO proteomics. Nat Rev Mol Cell Biol 17, 581–595 [PubMed: 27435506]
46. Liu S, Sheng H, Yu Z, Paschen W, and Yang W (2016) O-linked beta-N-acetylglucosamine modification of proteins is activated in post-ischemic brains of young but not aged mice: Implications for impaired functional recovery from ischemic stress. J Cereb Blood Flow Metab 36, 393–398 [PubMed: 26661187]

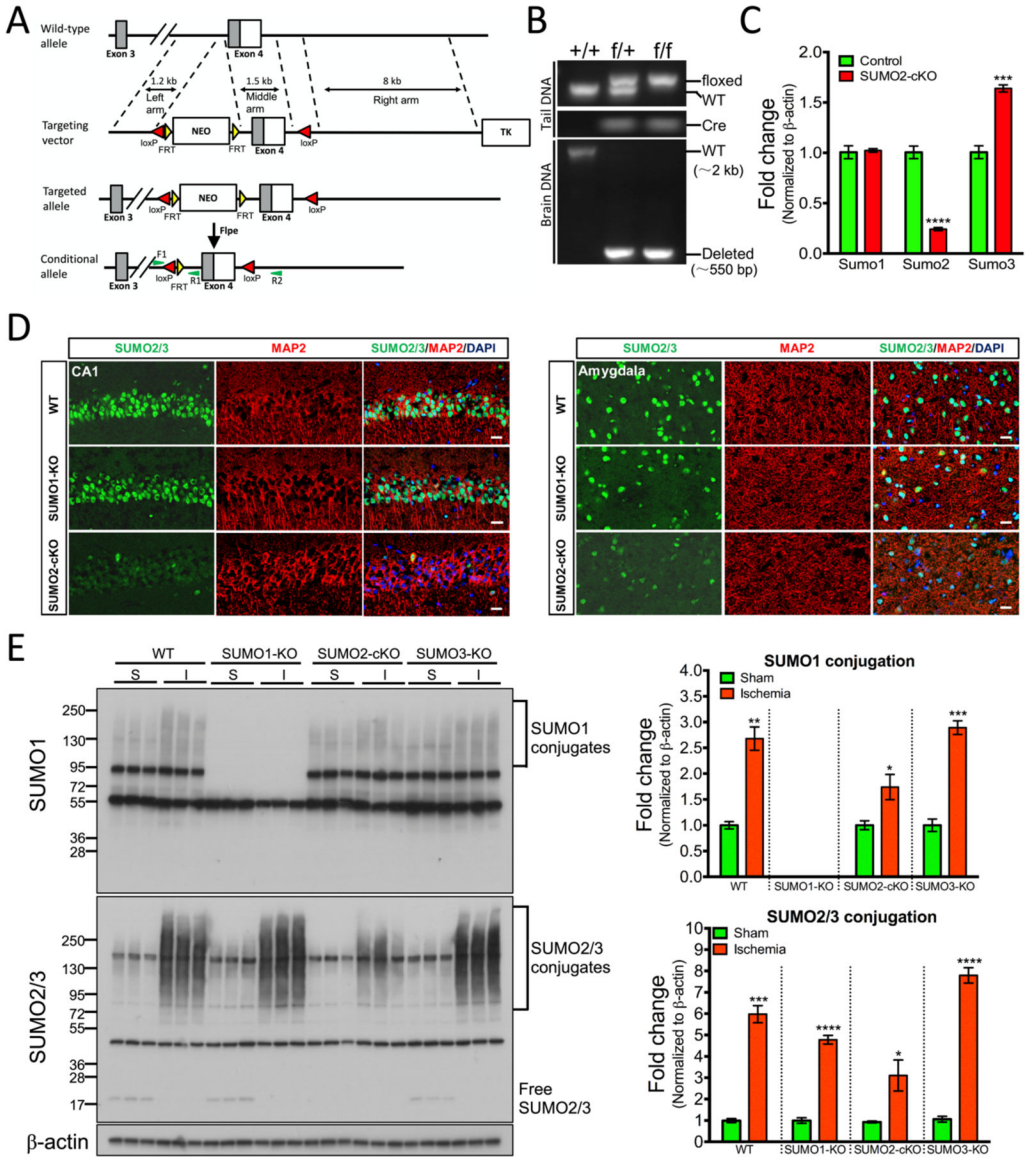

Figure 1. Generation and characterization of conditional *Sumo2* knockout mice.

A) Targeting strategy for conditional deletion of exon 4 of the *Sumo2* gene. The targeting vector was designed to introduce an FRT-flanked neomycin cassette (NEO) and 2 loxP sites into the targeted locus. After removal of the NEO cassette, the *Sumo2*$^{f/f}$ mouse line was obtained. Gray rectangles, coding exons; red triangle, loxP site; yellow triangle, FRT site; green arrow, primers (F1 and R1 for genotyping; F1 and R2 for verification of exon 4 deletion); TK, thymidine kinase cassette. Not drawn to scale. **B,C)** Deletion of *Sumo2* in the mouse brain. *Sumo2*$^{f/f}$ mice were crossed with Emx1$^{Cre/Cre}$ mice to generate *Sumo2*$^{f/f}$;Emx1-Cre mice (SUMO2-cKO). Genotyping pri**B)** Verification of deletion of *Sumo2* exon 4 in the SUMO2-cKO mouse brain using brain DNA samples. **C)** Quantitative RT-PCR analysis of SUMO1–3 expression in the hippocampus of control and SUMO2-cKO mice. **D,E)** SUMOylation dynamics in response to ischemic stress in the brain. **D)** Immunohistochemical analyses of SUMO2/3 and MAP2 expression in CA1 hippocampus

and amygdala. Mice were subjected to 8 minutes of global brain ischemia and 1 hour of reperfusion. Brain sections were stained with anti-SUMO2/3 and anti-MAP2 (neuronal marker) antibodies. WT, wild-type. Scale bars: 20 μm. **E)** Wild-type (WT), SUMO1-KO, SUMO2-cKO, and SUMO3-KO mice were subjected to sham surgery (S) or 10 minutes forebrain ischemia (I) and 1 hour reperfusion. The ischemia-induced changes in global SUMOylation were evaluated by Western blotting. The high-molecular-weight regions, marked by brackets, were used to quantify SUMO1 and SUMO2/3 conjugation. Signal intensities were normalized to β-actin. To calculate fold change, mean values of the WT/sham group were set to 1.0. Data are presented as means ± SEM (n = 3/group). *$p < 0.05$; **$p < 0.01$; ***$p < 0.001$; ****$p < 0.0001$, vs respective sham group.

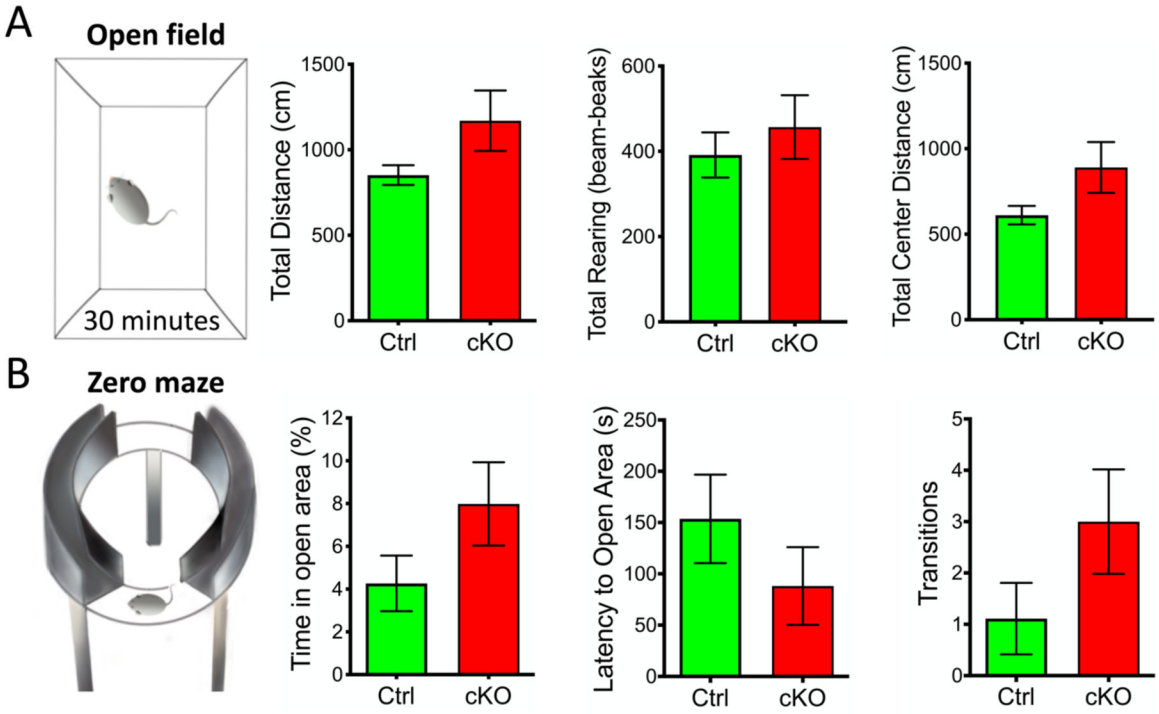

Figure 2. Open field and elevated zero maze tests.

These tests were conducted with control (Ctrl) and SUMO2-cKO (cKO) mice. **A)** Open field activity for locomotion (*left*), rearing (*middle*), and distance traveled in the center zone (*right*). No significant genotype effects were found in any of the analyses. Control vs. SUMO2-cKO: locomotion [$t(1,15) = -1.799$, $p = 0.092$], rearing [$t(1,15) = -0.725$, $p = 0.480$]; and center distance [$t(1,15) = -1.846$, $p = 0.085$]. **B)** Elevated zero maze performance depicting percent time in open areas (*left*), latency to enter open areas (*middle*), and numbers of transitions from closed-to-open-to-closed areas (*right*). Control vs. SUMO2-cKO: percent time [$t(1,15) = -1.623$, $p = 0.125$], latency [$t(1,15) = 1.127$, $p = 0.278$], and transitions [$t(1,15) = -1.562$, $p = 0.139$]. Data are presented as means ± SEM (n = 8–10 mice/genotype).

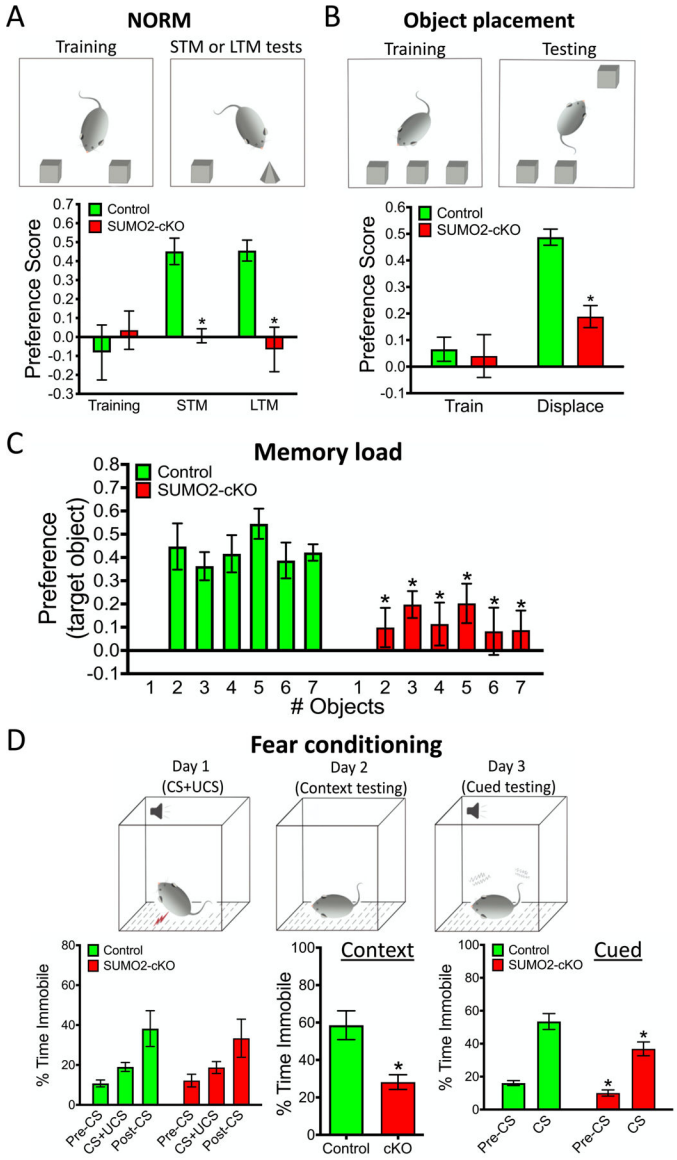

Figure 3. Cognitive tests in SUMO2-cKO mice.

A) Preference scores in the novel object recognition memory (NORM) test depicting training, short-term memory (STM) and long-term memory (LTM) testing. RMANOVA for object preference revealed significant within subjects effects of time [$F(2,36)=3.468$, $p=0.042$] and a significant time by genotype interaction [$F(2,36)=5.655$, $p=0.007$]. The between subjects effects of genotype was significant [$F(1,18)=21.333$, $p<0.001$]. n = 8–10 mice/genotype. **B)** Preference scores for the displaced object in the spatial object task. The RMANOVA revealed significant trial effects (training and test) [$F(1,15) = 32.910$, $p < 0.001$], a trial by genotype interaction [$F(1,15) = 24.175$, $p < 0.001$], and a genotype effect [$F(1,15) = 4.728$, $p = 0.046$]. **C)** Preference scores for the novel object in the memory load test. The RMANOVA revealed a significant trials effect (trials 1–7) [$F(6,90) = 5.870$, $p < 0.001$], trials by genotype interaction [$F(6,90) = 1.888$, $p = 0.093$], and genotype effect [$F(1,15) = 23.046$, $p < 0.001$]. **D)** Fear conditioning. SUMO2-cKO mice were deficient in

contextual and cued fear conditioning. (*Left*) RMANOVA for conditioning revealed a significant time effect [$F(2,30) = 12.369$, $p < 0.001$]; however, the time by genotype interaction [$F(2,30)=0.208$, $p=0.813$] and the genotype effect [$F(1,15)=0.047$, $p=0.831$] were not significant. (*Middle*) Contextual fear was significant [$t(1,15) = 3.382$, $p = 0.004$]. (*Right*) RMANOVA for cued fear revealed significant time [$F(1,15) = 119.492$, $p < 0.001$] and genotype effects [$F(1,15) = 8.364$, $p = 0.011$]; the time by genotype interaction [$F(1,15)=3.243$, $p=0.092$] was not significant. Results shown as means ± SEM (n = 8–9 mice/genotype for panels B-D). *$p < 0.05$, compared to the respective controls.

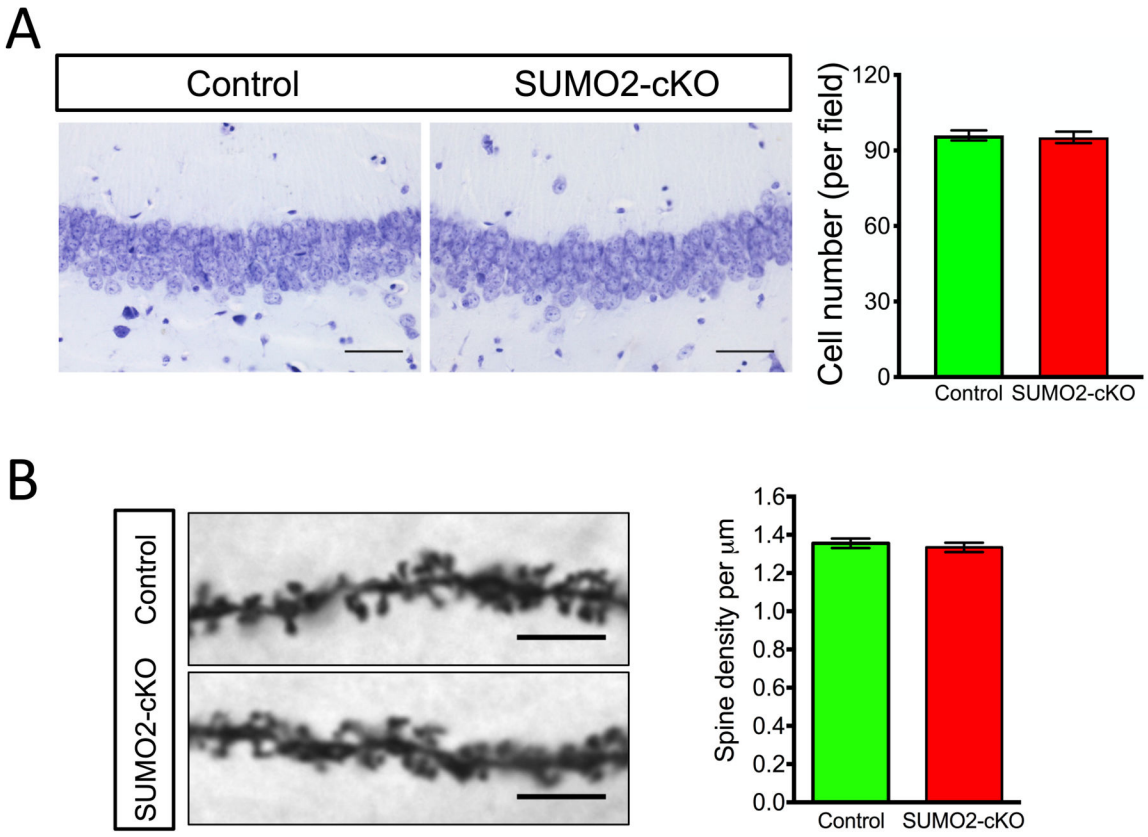

Figure 4. Cell numbers and spine densities in CA1 hippocampus of SUMO2-cKO mice.

A) No differences in cell numbers in hippocampus were observed between and control and SUMO2-cKO mouse brains (5 sections from each of 2 mice/group). Scale bars: 50 µm. **B)** No significant differences in spine densities of CA1 neurons were observed between control and SUMO2-cKO (40–50 neurons per animal; n = 3 per group). Scale bars: 5 µm.

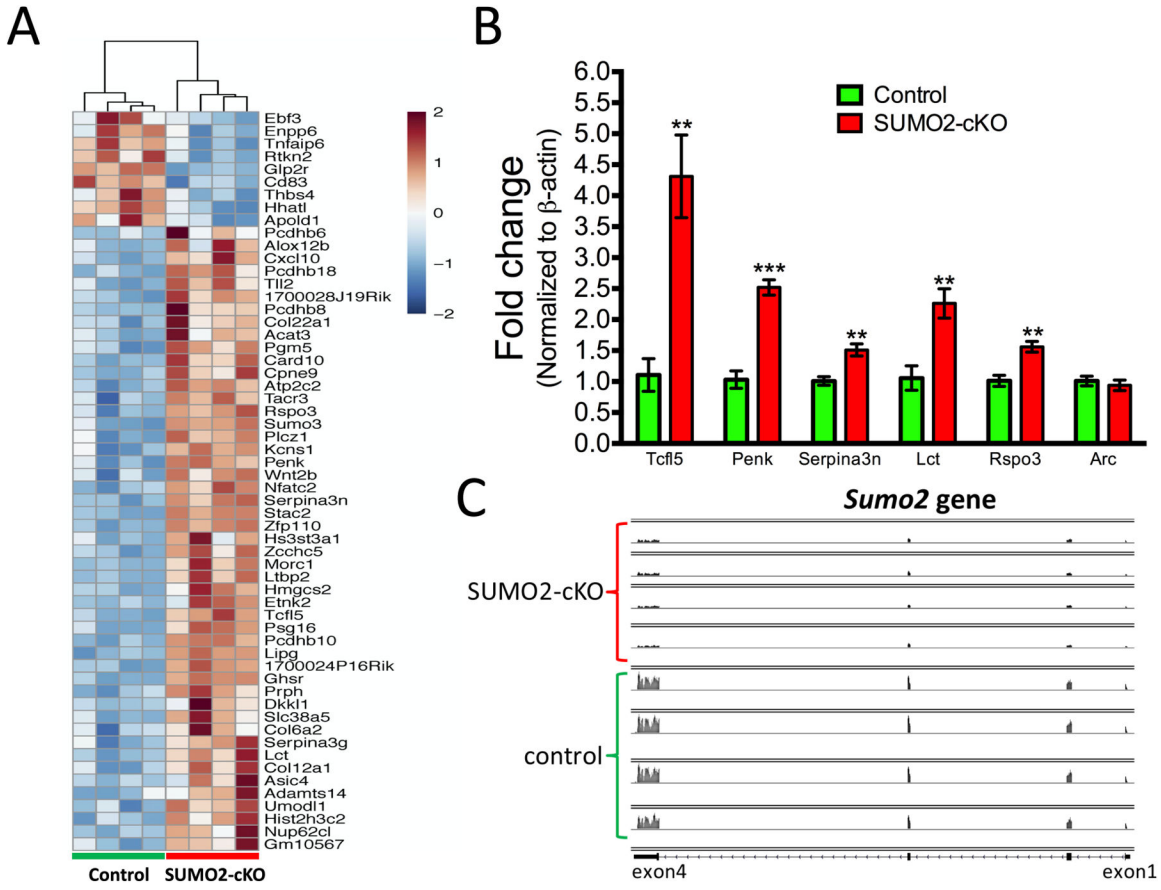

Figure 5. RNA-Seq analyses of hippocampal samples from control and SUMO2-cKO mice.

A) RNA-Seq gene expression heat map. RNA hippocampal samples were prepared from control and SUMO2-cKO mice. Differentially regulated genes (SUMO2-cKO vs control; Table S5) were used to generate the heat map. Heat map colors indicate the extent of fold changes between SUMO2-cKO vs control samples. **B)** Verification of RNA-Seq data by quantitative RT-PCR analysis. All data were normalized to β-actin. To calculate fold change, the mean values of control samples were set to 1.0. Data are presented as means ± SEM (n=3/group); $^{**}p < 0.01$; $^{***}p < 0.001$, cKO versus control. **C)** Read coverage across the *Sumo2* gene in both genotypes. Reads were aligned to multiple genomic positions using the STAR alignment algorithm. Illustration of the *Sumo2* gene, including its exons and introns, is shown at the bottom. Note that the number of reads is dramatically reduced in SUMO2-cKO vs control.

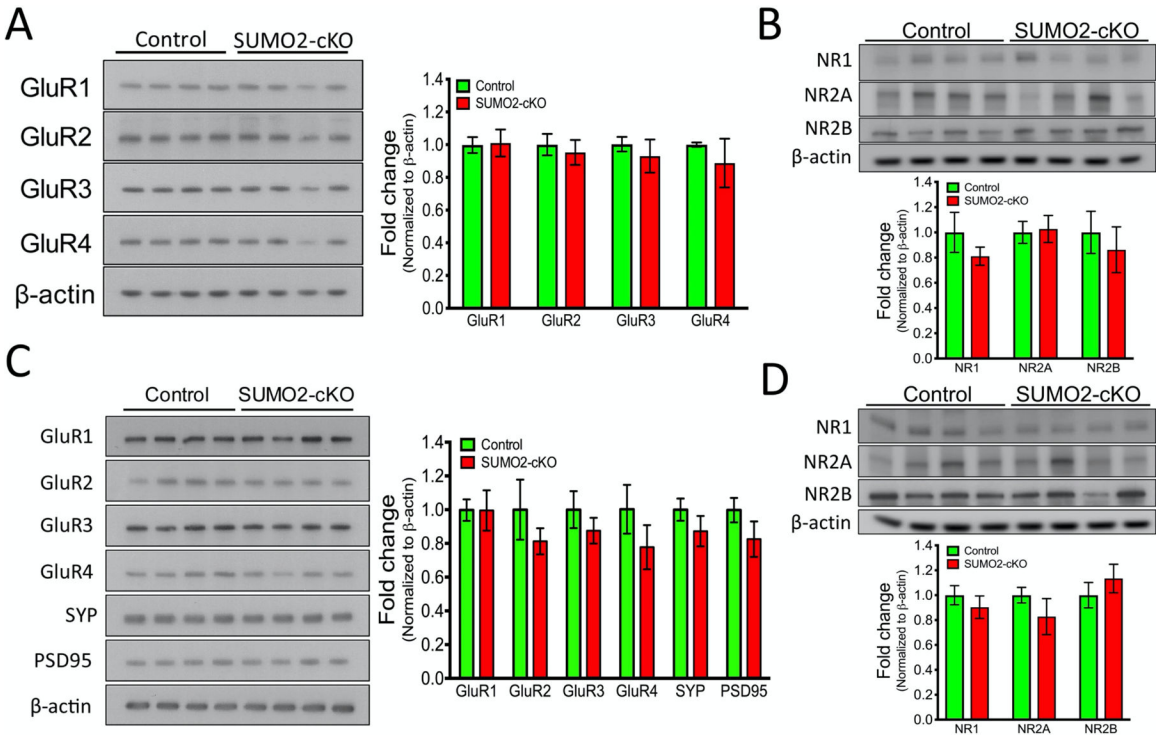

Figure 6. Western blot analysis of hippocampal samples from control and SUMO2-cKO mice.

Levels of AMPA receptors (GluR1–4), NMDA receptors (NR1, NR2A, and NR2B) and other memory-related proteins, including synaptophysin (SYP) and PSD95, were evaluated using tissue homogenates **(A,B)** and synaptosome fractions **(C,D)** from hippocampus. Quantitative data from Western blotting were generated by normalizing the intensities of each band to β-actin. Mean values of the control group were set to 1.0. Data are presented as means ± SEM (n=4/group).

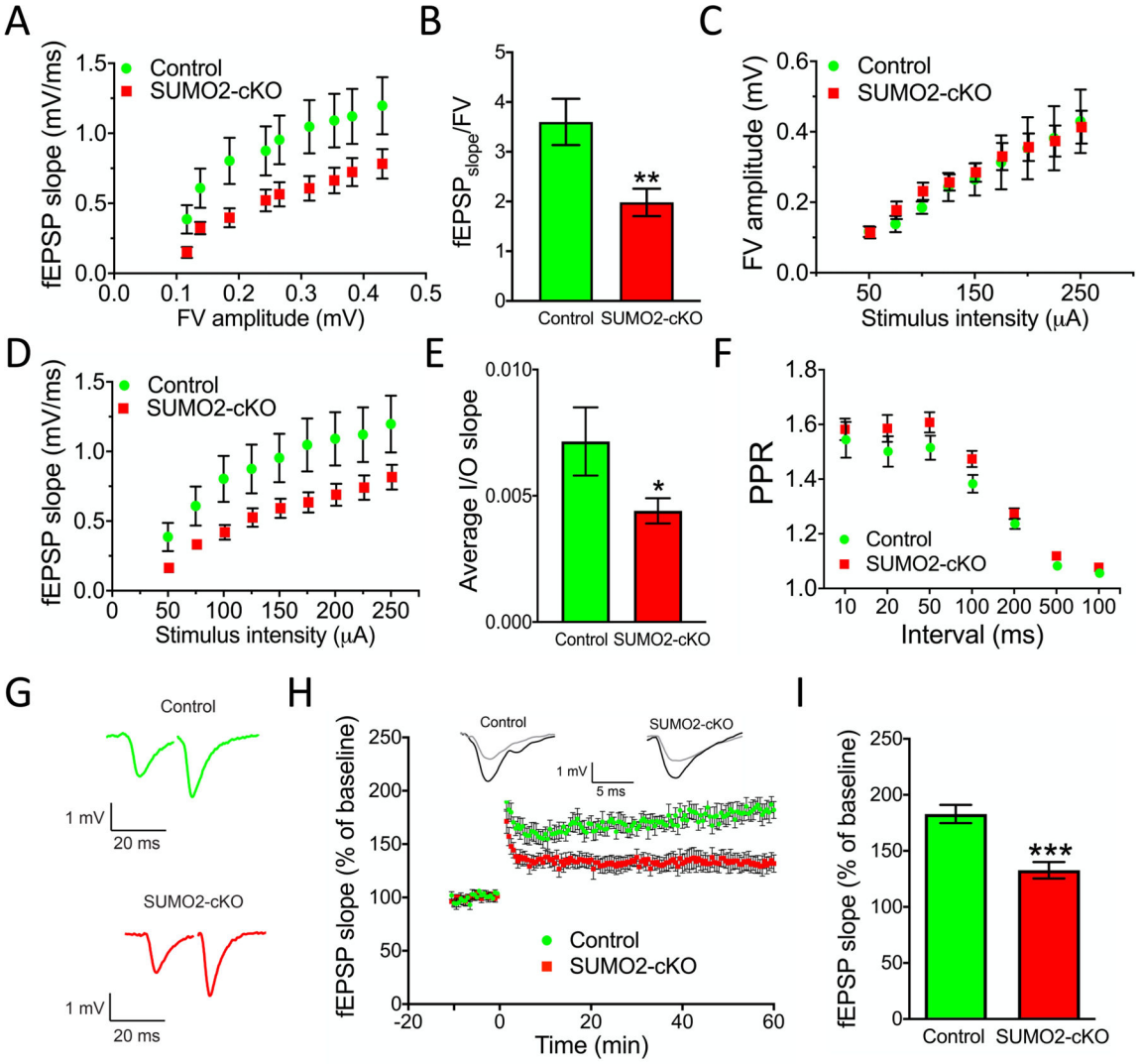

Figure 7. CA1 hippocampal synaptic transmission in SUMO2-cKO mice.

A) Input–output curve showing the relationship between pre-synaptic axonal fiber volley (FV) amplitude and fEPSP slope (in the range of 50 to 250 μA stimulation) RMANOVA revealed significant main effects of FV [$F(9, 108) = 77.04$, $p<0.0001$], genotype [$F(1, 12) = 4.846$, $p=0.048$], and the intensity by genotype interaction [$F(9, 108) = 3.52$, $p=0.0007$] (n=6–8 slices/group). **B)** The mean ratio of the FV-fEPSP slope was significantly reduced in SUMO2-cKO mice compared to littermate controls [$t(1,12)=3.166$, $p=0.008$] (n=6–8 slices/group). **C)** The relationship between FV amplitude and stimulus intensity was similar in SUMO2-cKO and control mice. RMANOVA revealed significant main effects of intensity [$F(9, 108) = 47.93$, $p<0.0001$], but genotype was not a significant factor [$F(1, 12) = 0.047$, $p=0.833$], and the intensity by genotype interaction was also not significant [$F(9, 108) = 0.287$, $p=0.977$] (n=6–8 slices/group). **D**) fEPSP slope amplitude in response to increasing stimulus intensity. RMANOVA revealed significant main effects of intensity [$F(9,117) = 87.04$, $p<0.0001$], genotype [$F(1,13) = 5.267$, $p=0.039$], and the intensity by genotype interaction [$F(9,117) = 3.747$, $p=0.0004$] (n=6–9 slices/group). **E)** The mean I/O slopes in SUMO2-cKO were significantly smaller relative to control mice [$t(1,13)=2.407$, $p=0.032$].

F) Paired-pulse facilitation was similar between genotypes. Mean responses at different stimulus intervals. **G)** Examples of traces showing responses to pairs of pulses at a 20 millisecond (ms) intervals. **H)** The mean time-course of fEPSP before and after induction of long-term potentiation (LTP) at time 0, expressed as the percent fEPSP slope normalized to a 10-minute baseline. *Inset:* representative traces of fEPSPs before (*gray line*) and 60 minutes after (*black line*) LTP induction. **I)** Percent fEPSP slope potentiation 60 minutes after LTP induction; mean slopes values for each experimental group consisted of 10 consecutive recordings (55–60 minutes post high frequency stimulation) and were significantly different between genotypes [$t(1,13)=4.582$, $p=0.0005$] (n = 7–8 slices/group). Data are presented as means ± SEM. *, $p < 0.05$; **, $p < 0.01$ ***, $p < 0.001$. fEPSP, field excitatory postsynaptic potential; presynaptic fiber volley (FV); PPR, paired pulse ratio.